Electrochimica Acta 81 (2012) 64–73

Contents lists available at SciVerse ScienceDirect

Electrochimica Acta

journal homepage: www.elsevier.com/locate/electacta

A study on molybdenum sulphoselenide (MoS_xSe_{2-x}, $0 \le x \le 2$) thin films: Growth from solution and its properties

T. Joseph Sahaya Anand*, S. Shariza

Department of Engineering Materials, Faculty of Manufacturing Engineering, Universiti Teknikal Malaysia Melaka, Durian Tunggal, 76100 Melaka, Malaysia

ARTICLE INFO

Article history:
Received 2 March 2012
Received in revised form 19 July 2012
Accepted 21 July 2012
Available online xxx

Keywords:
Molybdenum sulphoselenide
Thin films
Electrodeposition
Direct bandgap
Mott–Schottky plots

ABSTRACT

Thin films of molybdenum sulphoselenide, MoS_xSe_{2-x}, $(0 \le x \le 2)$ have been electrosynthesized on indium-tin-oxide (ITO)-coated glass and stainless steel substrates. The films were characterized for their structural, morphological and compositional characteristics. Their optical and semiconducting parameters were also analysed in order to determine the suitability of the thin films for photoelectrochemical (PEC)/solar cell applications. Structural analysis via X-ray diffraction (XRD) analysis reveals that the films are polycrystalline in nature. Scanning electron microscope (SEM) studies reveals the films were adherent to the substrate with uniform in nature which also confirmed by Transmission electron microscope (TEM). Compositional analysis via energy dispersive X-ray (EDX) technique confirms the presence of Mo, S and Se elements in the films. The optical studies show that the films are of direct bandgap. Results on the semiconductor parameters analysis of the films showed that the nature of the Mott–Schottky plots indicates that the films obtained are of n-type material. For all films, the semiconductor parameter values come in the better range of other transition metal chalcogenides which has proven that MoSSe thin films are capable as solar/PEC cell materials.

1. Introduction

Transition metal chalcogenides (TMCs) are semiconductors, which can be used as an efficient photovoltaic material. Promising results have been obtained in the realization of photoelectrical solid-state device or solar cells by using TMC crystals [1–3]. Due to its significant characteristics by optical and semiconducting properties, transition metal chalcogenide compounds, especially in thin film form were discovered to be the right material in the photovoltaic industry for the development of photoelectrochemical (PEC) and solar cell panels [4–6]. These advancements have been proven by the vast number of research publications especially in the last decade, on the application of TMC compounds in the PEC and solar cell industry [1–6].

For many applications, thin layers of TMC materials on substrates are required. There are quite a number of methods of preparing such layers, such as by spray pyrolysis, electrochemical deposition, sputtering etc. [1,3,5]. One of the attractive methods for producing thin films, owing to the possibility of large area deposition at low cost is the electrodeposition method. This method requires the presence of reagents that act as a source of chalcogenide and complexion of metal ions of interest whose stability equilibrium provide a concentration of metal cation small enough to produce the controlled homogenous precipitation of the film on the solid substrate [7]. Films prepared by this method can be used in high performance devices due to high purity of deposited material.

Of the many TMCs, transition metal chalcogenides (MX_2) where M = Mo and X = S and Se having MoS_2 and $MoSe_2$ type structure have been widely used for solar energy conversion in PEC solar cells [7,8]. The dichalcogenides of Mo attracted considerable interest due to their well matched band gap (E_g) with solar spectrum as well as due to unique layer lattice structures. Hence, we propose in this investigation the synthesis, growth mechanism, optical and semiconducting properties of combinatorial molybdenum sulphoselenide MoS_xSe_{2-x} $(0 \le x \le 2)$ thin films. Based on the optical gap of these materials and that the optical gaps could be engineered, it is proposed in these investigations to synthesize alloyed material in thin film form and to characterize it through the optical and electrical properties with special reference to the film composition. The studies include the observations on growth kinetics, structural, morphological, compositional, optical and semiconducting parameters of these films.

2. Experimental details

2.1. Preparation of thin films

The precursors molybdic acid (H_2MoO_4), sodium thiosulphate pentahydrate ($Na_2S_2O_3{\cdot}5H_2O$) and selenium dioxide (SeO_2) of analytical grade were used as Mo^{4+}, S^{2-} and Se^{2-} ion sources,

* Corresponding author. Tel.: +60 6 331 6489; fax: +60 6 331 6411.
E-mail address: anand@utem.edu.my (T.J.S. Anand).

0013-4686/$ – see front matter © 2012 Elsevier Ltd. All rights reserved.
http://dx.doi.org/10.1016/j.electacta.2012.07.077

respectively. ITO glass and stainless steel substrates of dimension 15 mm × 25 mm × 1 mm size were cleaned before film deposition. ITO glass were dipped into diluted hydrochloric acid (HCl), rinsed with double distilled water then cleaned in hot air while stainless steel substrates were mirror polished and finally cleaned in an ultrasonic cleaner. This treatment increases the adhesion of the electrodeposits to the substrate and allows thicker deposition without peeling.

To prepare the electrolyte solutions having relative concentrations of 0.5 M H_2MoO_4, 0.5 M SeO_2 and 0.5 M $Na_2S_2O_3{\cdot}5H_2O$, the following solutions were first prepared: solution A containing H_2MoO_4 in ammonia, solution B containing $Na_2S_2O_3{\cdot}5H_2O$ and solution C containing SeO_2 in distilled water. These solutions were mixed in proportional amounts as the precursor electrolyte. For the synthesis of $MoSe_2$ ($x=0$) and MoS_2 ($x=2$), the electrolyte mixture ratio between the precursor solutions of H_2MoO_4 and $Na_2S_2O_3{\cdot}5H_2O$ or SeO_2 (where applicable) was selected to be 1:2 following its stoichiometry. For synthesis of MoSSe ($x=1$), the ratio of precursors H_2MoO_4:SeO_2:$Na_2S_2O_3{\cdot}5H_2O$ was adjusted to 1:1:1 accordingly. The pH of the reactive mixture is set at ~pH 10 by adding drops of NaOH to the mixture. After mixing for 5 min under stirring and heating to reach a reaction temperature of 40 ± 1 °C, the mixture is ready for synthesis of the films. A Princeton Applied Research Model VersaSTAT 3 Potentiostat was employed for the electrodeposition of the films. The deposition potential for the chalcogenide thin film was first derived from cyclic voltammetry (CV) technique followed by synthesis of the chalcogenides by electrodeposition technique. In the case for transition metal chalcogenide compounds, the potential limit range −1.00 V to 1.00 V was found to be suitable [9,10] for CV measurements. A three-electrode cell system was adopted for the CV measurement and electrodeposition of the film in a manner described in [11]. The films were deposited at different periods of time ranging from 10 to 30 min with 5 min time interval.

2.2. Characterization of electrodeposited thin films

Film thickness of MoS_xSe_{2-x} ($0 \le x \le 2$) was determined by gravimetric weight difference method using a sensitive microbalance and assuming film density as the bulk density of the compounds. X-ray diffraction (XRD) and scanning election microscopy (SEM) analysis were performed by using PANalytical ZPERT PROMPD PW 3040/60 diffractometer (for 2θ range from 20 to 80° with CuK_α radiation) and SEM ZEIZZ EVO 50 scanning microscope, respectively and its composition analysis with energy dispersive X-ray (EDX) analysis. JEOL 2000-FX TEM operated at 200 kV was used for TEM analysis. Optical properties for determination of energy band gap of the films and semiconductor properties of the films related to its possible application in the photoelectrochemical (PEC)/solar cell were studied using UV–vis spectrophotometer and Mott–Schottky plot analysis, respectively.

3. Results and discussion

3.1. Kinetics and growth mechanism

Thin film formation of MoS_xSe_{2-x} ($0 \le x \le 2$) occurs as a result of the various chemical reactions taking place in the deposition bath. In the present investigation ionic species of molybdenum, sulphide and selenide are produced by the following reaction equilibria in an aqueous alkaline deposition bath.

$$H_2MoO_4 + 6H^+ + 2e^- \rightarrow Mo^{4+} + 4H_2O \quad (1)$$

$$SeO_2 + H_2O \rightarrow H_2SeO_3$$

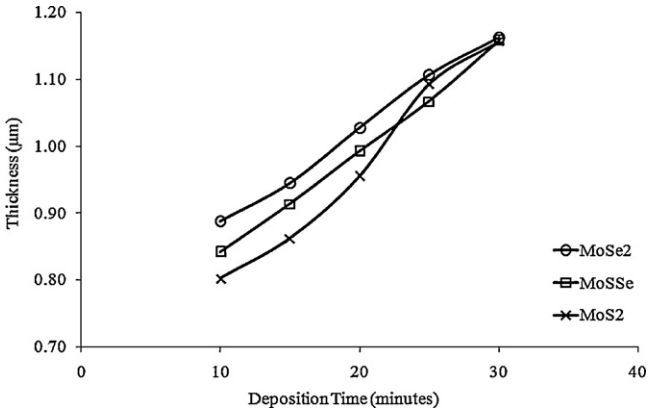

Fig. 1. Variation of thickness with deposition time for the electrodeposited thin films.

On the substrate surface, H_2SeO_3 reduces to selenium:

$$H_2SeO_3 + 4H^+ + 6e^- \rightarrow Se^{2-} + 3H_2O \quad (2)$$

$$Na_2S_2O_3 \leftrightarrow Na^{2+} + {S_2O_3}^{2-}$$

$${S_2O_3}^{2-} + 6H^+ + 6e^- \leftrightarrow 2S^{2-} + 3H_2O \quad (3)$$

Reaction (1) shows that metal ions are produced by dissociation of the metal complex while chalcogenide ions (Reactions (2) and (3)) are produced by dissociation of sulphur and selenium precursors in the aqueous alkaline medium. When the concentration of ionic species Mo^{4+}, S^{2-} and Se^{2-} exceeds in the reaction bath, nucleation starts which results in growth of molybdenum sulphoselenide, MoS_xSe_{2-x} ($0 \le x \le 2$) thin films. The as-reduced Mo, Se and S atoms are very active and can easily combine to produce MoS_xSe_{2-x} ($0 \le x \le 2$) compound. The kinetics growth of film can be understood from the following:

If $x=0$, $MoSe_2$ formation:

$$Mo^{4+} + 2Se^{2-} \rightarrow \underset{\text{molybdenum diselenide}}{MoSe_2} \quad (4)$$

If $x=1$, MoSSe formation:

$$Mo^{4+} + Se^{2-} + S^{2-} \rightarrow \underset{\text{molybdenum sulphoselenide}}{MoSSe} \quad (5)$$

If $x=2$, MoS_2 formation:

$$Mo^{4+} + 2S^{2-} \rightarrow \underset{\text{molybdenum disulphide}}{MoS_2} \quad (6)$$

The growth of the films was studied through the film thickness plot in Fig. 1. It shows an initial induction period of about 10 min, where no clearly observable growth occurs. In this period, a very thin and almost no film formation is observed. Thereafter, the film begins to form. The presence of initial induction period can be attributed to the growth mechanism where nucleation occurs first followed by the combination of ions for the subsequent linear film growth [12]. This is the evidence of a typical 'ion-by-ion' growth mechanism. The resultant films were homogenous, well adherent to the substrates and uniform to the naked eye. There is a prominent increase in thickness of the MoS_2 film at time 25 min. This particular observation leads to the phenomena whereby, at 25 min, the MoSSe film is thinner than the MoS_2 film. This does not fit into the general trend of the thickness of $MoSe_2$ > MoSSe > MoS_2 films. At this point, the rate of yielding the ternary MoSSe film was lower than normal due to the complexity of growth a ternary compound.

Table 1
Comparison of experimental '*d*' values with JCPDS data for $MoSe_2$, MoSSe and MoS_2 thin films.

Material	Angle (2θ)	($h\,k\,l$)	Standard (Å)	Experimental (Å)				
			'*d*'$_{JCPDS}$	10 min	15 min	20 min	25 min	30 min
$MoSe_2$	31.70	(1 0 1)	2.8206	3.0153	2.8189	2.7241	2.8738	3.0231
	39.19	(0 1 5)	2.2971	–	–	–	2.2634	2.2657
	45.62	(1 0 7)	1.9868	2.0323	2.0351	2.0299	2.0340	2.0117
	49.31	(0 1 8)	1.8467	1.8003	1.7968	1.8004	1.8009	1.7998
MoSSe	44.49	(1 2 –4)	2.0348	–	–	2.0365	2.0339	2.0347
	50.62	(1 4 0)	1.8015	1.8097	1.8022	1.8009	1.8007	1.7994
MoS_2	44.37	(1 0 4)	2.0400	–	2.0345	2.0331	2.0383	2.0334
	50.08	(1 0 5)	1.8200	1.7985	1.8027	1.8017	1.7961	1.8006

3.2. Structural characterization

The structural characterization via XRD measurement with a diffractogram, showing phases present (peak positions), phase concentrations (peak heights), amorphous content (background hump) and crystallite size/strain (peak widths) [13]. All standard and experimental '*d*' spacing values with reference to JCPDS cards are summarized in Table 1. Peaks belonging to $MoSe_2$ are detected for the films prepared at all the deposition times investigated as shown in Fig. 2. The peaks are identified as (1 0 1), (0 1 5), (1 0 7) and (0 1 8) planes of $MoSe_2$ and (1 1 1) and (2 2 0) planes of the stainless steel substrate [14]. The structural features fit into the rhombohedral structure of the $MoSe_2$ films with lattice parameter values $a = b = 0.3292$ nm and $c = 1.9392$ nm which is in good agreement with the standard values [15]. Peaks of $MoSe_2$ at $2\theta = 29.5^\circ$ and 45.1° become more prominent indicating that the (1 0 1) and (1 0 7) plane films grow with time. Also, at deposition time 25 min and 30 min, a $MoSe_2$ film having (0 1 5) plane structure emerges at $2\theta = 39.8^\circ$. This shows that the super lattice peak (0 1 5) can be found only in thicker films.

Peaks belonging to MoSSe films deposited for a period of 10–30 min are detected and labelled accordingly in Fig. 3. At 20 min deposition time, a MoSSe peak at $2\theta = 44.5^\circ$ start to emerge and become more distinct from the neighbouring peak indicating that the super lattice peak (1 2 –4) grains can be found only in thicker films. The structural features fit into the rhombohedral structure of the MoSSe films with lattice parameter values $a = b = 0.9533$ nm and $c = 1.7363$ nm which is in good agreement with the standard values [16]. Fig. 4 shows the XRD patterns of MoS_2 films and the peaks are identified as (1 0 4) and (1 0 5) planes of MoS_2. The structural features fit into the hexagonal structure of the MoS_2 films with lattice parameter values $a = b = 0.3150$ nm and $c = 1.2300$ nm which is in good agreement with the standard values [17]. At 15 min deposition time, a MoS_2 peak at $2\theta = 44.4^\circ$ start to emerge and become more distinct from the neighbouring peak indicating that the (1 0 4) plane films grow with time. According to the Debye–Scherrer approach [18], the interplanar distances '*d*' corresponding to different ($h\,k\,l$) planes were calculated from the X-ray diffractograms. The crystallite size was calculated from the measurement of full-width at half-maximum (FWHM) in different X-ray peaks and values are in the range of 45–65 nm for $MoSe_2$ films, 44–55 nm for MoSSe films and 54–90 nm for MoS_2 films.

High-intensity peaks of diffractogram in Figs. 2–4 of the films reveal the completeness of crystallization process. This is due to the fact that the crystallinity increases with the increase of deposition time [19]. Enhancement of grain crystallinity with thickness, as presented in thickness measurement is due to increase in deposition time and growth mechanism involved in the film formation. The enhancement of microcrystalline growth that is initiated along

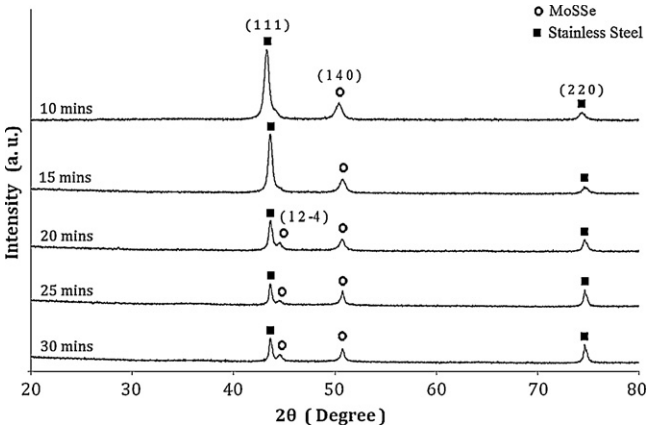

Fig. 3. XRD pattern for MoSSe thin films deposited at different deposition times.

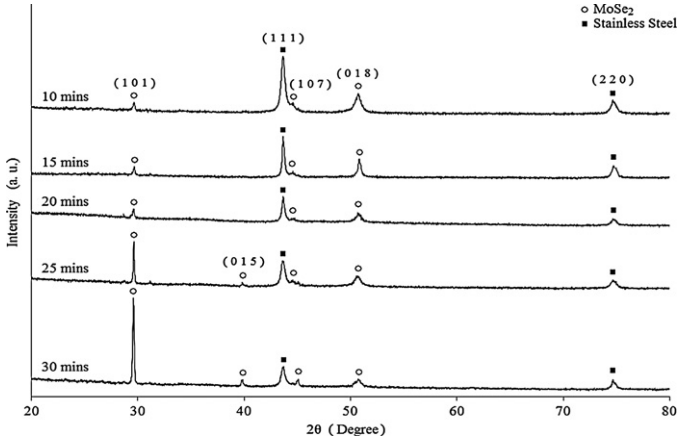

Fig. 2. XRD pattern for $MoSe_2$ thin films deposited at different deposition times.

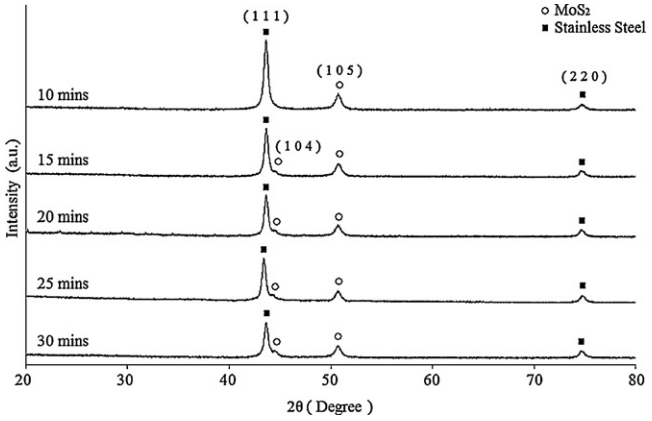

Fig. 4. XRD pattern for MoS_2 thin films deposited at different deposition times.

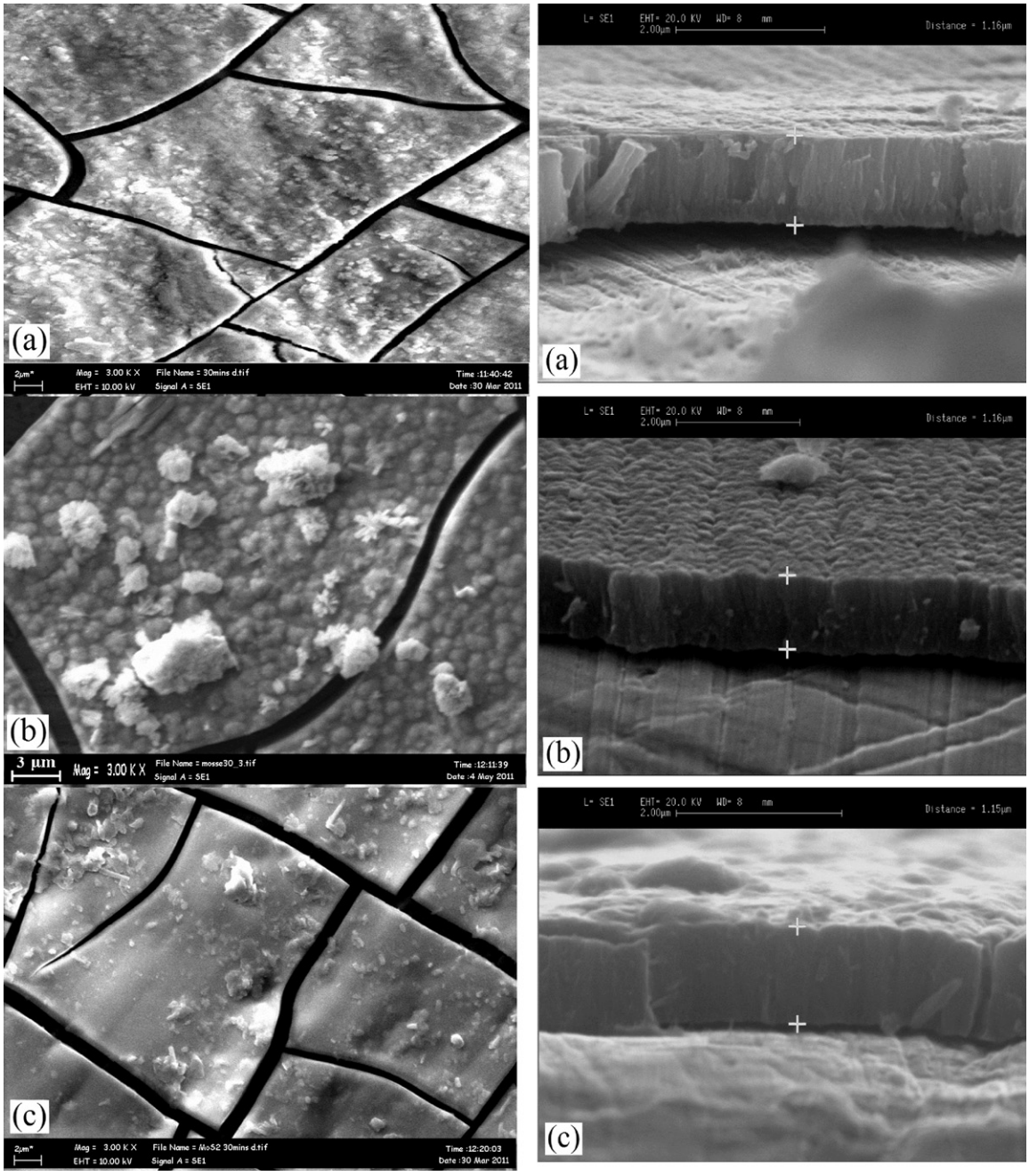

Fig. 5. SEM planar and cross sectional images of MoS_xSe_{2-x} $(0 \le x \le 2)$ films deposited at 30 min. (a) $MoSe_2$, (b) MoSSe and (c) MoS_2.

the substrate planes have resulted in some preferred orientation crystals to evolve only at longer deposition times. The preferred orientation is attributed to the enhancement in surface diffusion of the absorbed species with the increase of thickness resulting in an improvement in crystallinity of MoS_xSe_{2-x} $(0 \le x \le 2)$ thin films. In all films, the enhancement of the planes and the improved crystallinity with film thickness is remarkable irrespective of the electrolyte bath composition.

3.3. Morphological characterization

The surface morphology of MoS_xSe_{2-x} $(0 \le x \le 2)$ thin films deposited on stainless steel substrates of both planar and cross sectional images are shown in Fig. 5 for observation of film thickness deposited at 30 min. Unsymmetrical crystallites forms on ternary chalcogenide films as observed in MoSSe film is due the separation and precipitation of sulphide and selenide phases. The separation of chalcogenide phases is observable in ternary chalcogenide films as reported [20]. The morphology of the surface is better in films with selenium content. $MoSe_2$ film was observed to have smoother surface compared to MoSSe and MoS_2 films (whereby Se content is relatively less) which are also shown in plane-view TEM image (Fig. 6). This is due to better orientation of crystal in the films upon addition of selenium [20]. At longer deposition times, the structure of the films starts to break into grains (flakes) although still adhering to the substrate. The grains of the materials keeps on growing with time, causing the films to break and forming flake-like structures upon reaching the maximum grain stress point. The cracking

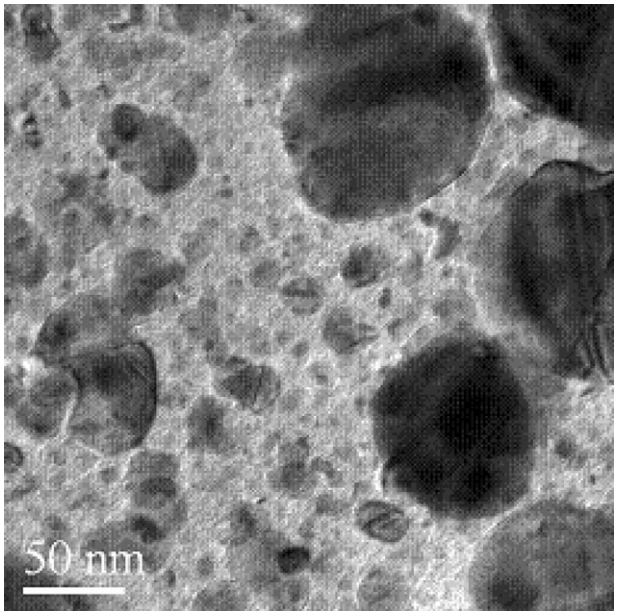

Fig. 6. Plane-view TEM bright field image of $MoSe_2$ film deposited at 30 min.

in thin films is attributed to drying shrinkage in this case of hydrous films. It has been reported that films having thickness greater than 0.2 mm are prone to cracking [21].

3.4. Compositional characterization

Fig. 7 shows the EDX patterns for MoS_xSe_{2-x} $(0 \le x \le 2)$ thin films deposited at 30 min. Referring to the spectra, strong peaks for Mo, S and Se were identified. It is confirmed that mixed combinatorial films of molybdenum sulphoselenide, MoS_xSe_{2-x} $(0 \le x \le 2)$ have been formed through the electrodeposition process. The overlapping peaks for Mo and S elements has been identified as a limitation

Table 2
Compositional study with TEM-EDX.

Thin films MoS_xSe_{2-x} $(0 \le x \le 2)$		Elements	wt% ratio	Formula
$x = 0$	$MoSe_2$	Mo:Se	31.20:60.49	$MoSe_{1.93}$
$x = 1$	MoSSe	Mo:S:Se	34.20:29.96:33.60	$Mo_{1.14}S_{1.00}Se_{1.12}$
$x = 2$	MoS_2	Mo:S	31.88:63.16	$MoS_{1.98}$

of the EDX technique due to the corresponding X-rays generated by emission from different energy-level shells (K, L and M). This observation can also be seen through the compositional analysis of TEM-EDX results as shown in Fig. 8. From the results obtained from TEM-EDX, is it positive that stoichiometric MoS_xSe_{2-x} $(0 \le x \le 2)$ thin films have been formed through electrodeposition as presented in Table 2. Although elements C and O do not play any role in the synthesis of the films, their peaks can be observed in the spectrum due to the particular advantage of EDX whereby it possesses the capability for detection of low atomic number elements such as carbon and oxygen, which are ubiquitous in our environment. Furthermore, inclusion of oxygen is observed for all the films because it is found to be unavoidable for chemically deposited films as testified [22,23]. This is true and accepted for all films synthesized.

3.5. Optical properties of electrodeposited thin films

From the transmittance spectrum obtained, the corresponding bandgap energy of the thin films was studied via analysis of the Tauc plot of the films. The resulting plot has a distinct linear regime which denotes the onset of absorption. Thus, extrapolating this linear region to the abscissa yields the energy of the optical band gap of the material. The optical transitions in transition metal chalcogenides films are found to be direct and allowed type [20,24]. Hence, a graph ($r = 2$ for allowed direct) of $(\alpha h\nu)^2$ vs. $h\nu$ is drawn and the optical bandgap energy has been estimated by extrapolating the straight line portion to cut the energy axis. A prominent feature that can be seen in the $(\alpha h\nu)^2$ vs. $h\nu$ plots is that the linear

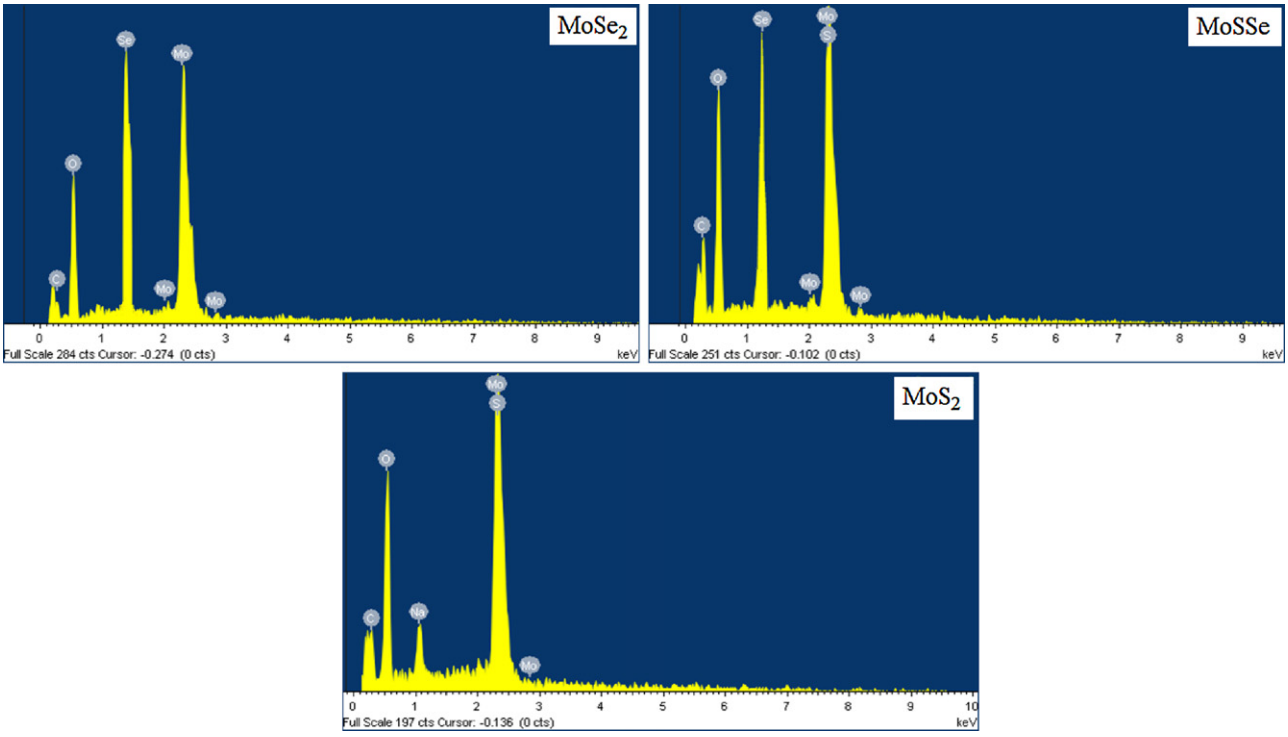

Fig. 7. EDX spectrum of electrodeposited MoS_xSe_{2-x} $(0 \le x \le 2)$ thin films.

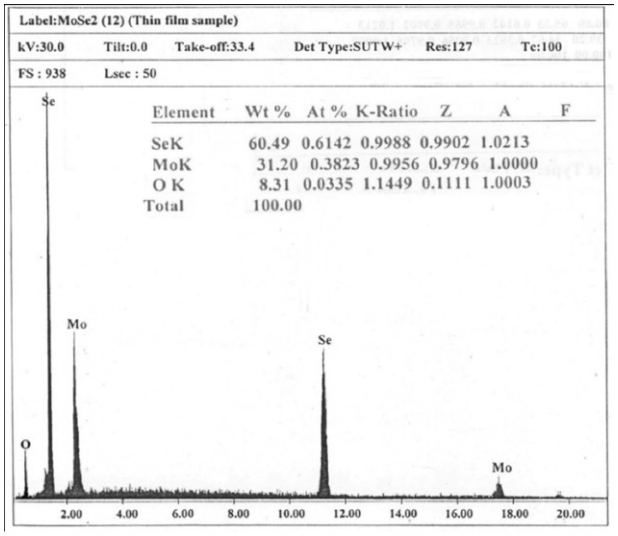

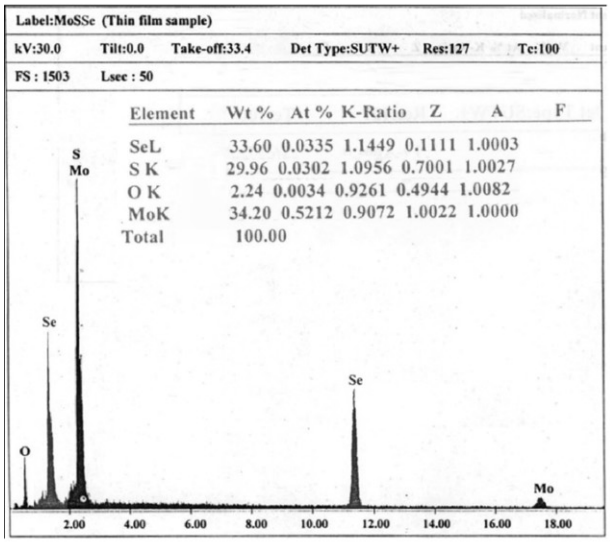

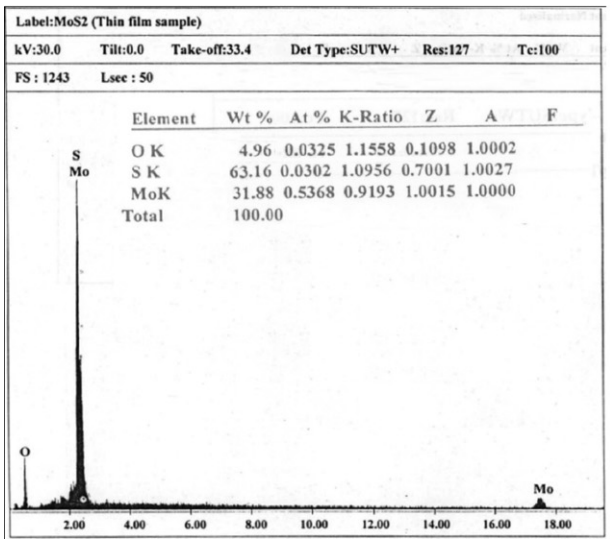

Fig. 8. TEM-EDX spectrum of electrodeposited MoS_xSe_{2-x} ($0 \le x \le 2$) thin films with compositional analysis.

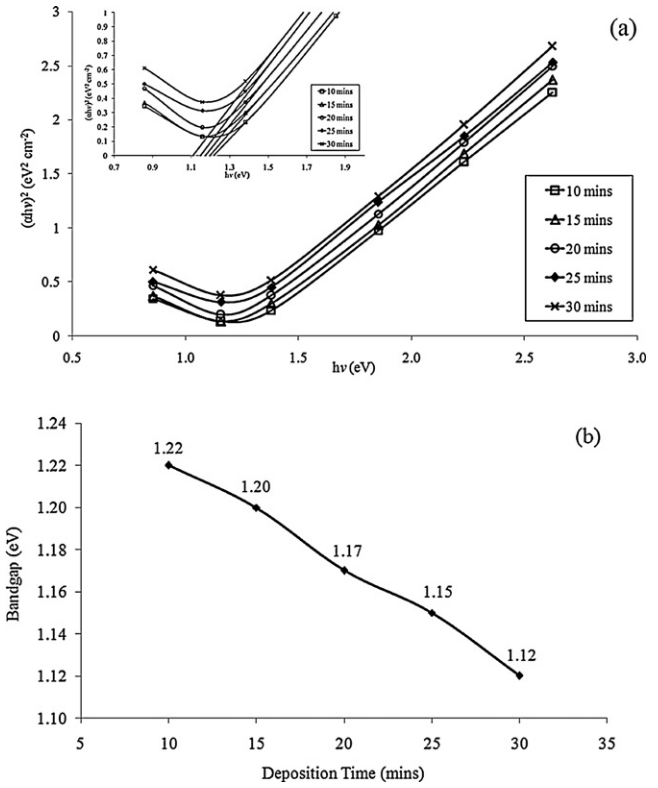

Fig. 9. Variation of $MoSe_2$ thin films deposited at different deposition times. (a) $(\alpha h\nu)^2$ vs. $h\nu$ and (b) bandgap vs. deposition time.

portion of the plot energy is greater than 2 eV. This is an indication of a direct transition type of material.

Fig. 9(a) shows the $(\alpha h\nu)^2$ vs. $h\nu$ plots of $MoSe_2$ thin films deposited at different deposition times (see inset graph). The variation of band gap energy (E_g) with the deposition time shows non-linear decrease is presented in Fig. 9(b). It is observed that with the increase of deposition time of the films, the E_g decreased from 1.22 to 1.12 eV, in good E_g range with the reported value [25] for $MoSe_2$ compound. As for MoSSe thin films, the $(\alpha h\nu)^2$ vs. $h\nu$ plots of MoSSe thin films deposited at different deposition times (see inset graph) is presented in Fig. 10(a). Following it, Fig. 10(b) depicts the variation of band gap energy (E_g) with the deposition time showing non-linear decrease. It is observed that with the increase of deposition time of the films, the E_g decreased from 1.66 to 1.44 eV, in good range with the reported value for molybdenum sulphoselenide thin films prepared by arrested precipitation technique (APT) [20].

On the other hand, for the MoS_2 thin films, the $(\alpha h\nu)^2$ vs. $h\nu$ plots of the deposited films at different deposition times is shown in Fig. 11(a) (see inset graph). Fig. 11(b) presents the non-linear decrease for the variation of band gap energy (E_g) with different deposition time. The figure shows that the E_g decreased from 1.74 to 1.64 eV with increase of deposition time for the MoS_2 thin films, in good range with the reported value [26] for MoS_2 compound. It is found that the bandgap of MoSSe films are intermediate between those of $MoSe_2$ and MoS_2. This can be understood due to the stoichiometry of the films. It can be concluded that the optical bandgap energy of all types of films decreases as the deposition time of the film increases. This result correlates to film thickness, whereby an increase in deposition time of the films result in greater thickness [27]. The corresponding values of the bandgap energy of the films with respect to film thickness are given in Table 3.

When the deposition conditions like substrate temperature of the film and solution concentration are kept fixed, the value of the band gap in general changes according to the thickness. The

Table 3
Bandgap energy values corresponding to film thickness of MoS_xSe_{2-x} ($0 \le x \le 2$) thin films.

Deposition time (min)	$MoSe_2$		MoSSe		MoS_2	
	Film thickness (μm)	Bandgap (eV)	Film thickness (μm)	Bandgap (eV)	Film thickness (μm)	Bandgap (eV)
10	0.8878	1.22	0.8423	1.66	0.8028	1.74
15	0.9449	1.20	0.9142	1.61	0.8624	1.72
20	1.0273	1.17	0.9923	1.54	0.9546	1.70
25	1.1070	1.15	1.0673	1.50	1.0927	1.67
30	1.1623	1.12	1.1582	1.44	1.1569	1.64

reasons for this change can be one of the following: (i) largeness of the dislocation, (ii) quantum size effect, (iii) changing barrier height because of variation in grain size in the polycrystalline film [28]. Only the third effect from these effects can cause an alteration in the values of the band gap of the deposited films. Contribution of the first effect can be very little, and the second one cannot be taken into account because the films are thick enough. The reason that we consider the third effect is that a decrease in barrier height is caused by an increase in grain size which in turn caused by an increase in film thickness. A decrease with an increase in thickness in direct band gap is also observed by many investigators [28,29]. The decrease in energy band gap after longer periods of deposition time is also attributed to improvement in the crystallinity as supported by the XRD studies. The time dependent parameters that affect the band gap are expected due to reorganization of the film and self-oxidation of the film. By filling the voids in the film as the deposition time increases, one expects denser films and smaller energy gaps.

3.6. Semiconductor parameters of electrodeposited thin films

A tabulation of the potential–capacitance behaviour data of MoSSe thin films for the system n-MoSSe|polyiodide|graphite electrode is done by plotting the inverse of the square of the capacitance vs. the applied potential to the films. In the Mott–Schottky graphs of $1/C^2$ sc vs. V_{SCE}, the voltage axis intercepts give the flat band potentials V_{FB}.

In terms of experimental voltages, the Mott Schottky equation is defined as:

$$\frac{1}{C^2} = \frac{2(V - V_{FB} - k_B T/e)}{\varepsilon \varepsilon_0 e N} \tag{7}$$

where C is the space charge capacitance, k_B is the Boltzmann's constant (1.38×10^{-23} J/K), T is the temperature of the operation (300 K), e is the electronic charge (1.603×10^{-19} C), ε is the dielectric constant of the film material, ε_o is the dielectric constant of free space (8.854×10^{-12} F/m) and N is the carrier concentration which is calculated from the slope of the graph.

The dielectric constants, ε for the films have been evaluated by using the relation:

$$\varepsilon = \frac{Cd}{A\varepsilon_0} \tag{8}$$

where C is the capacitance, d is the thickness of the crystal and A is the area of contact (2.25×10^{-6} m^2).

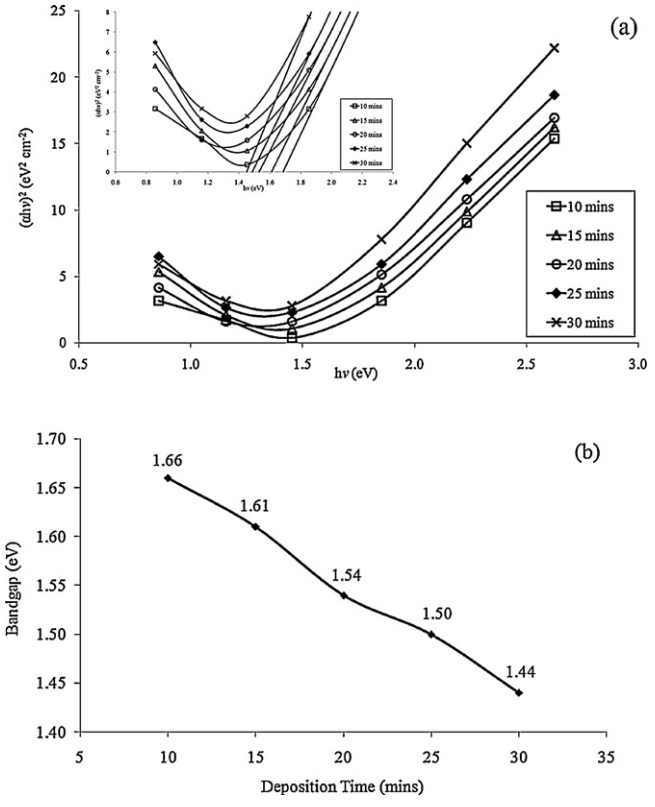

Fig. 10. Variation of MoSSe thin films deposited at different deposition times. (a) $(\alpha h\nu)^2$ vs. $h\nu$ and (b) bandgap vs. deposition time.

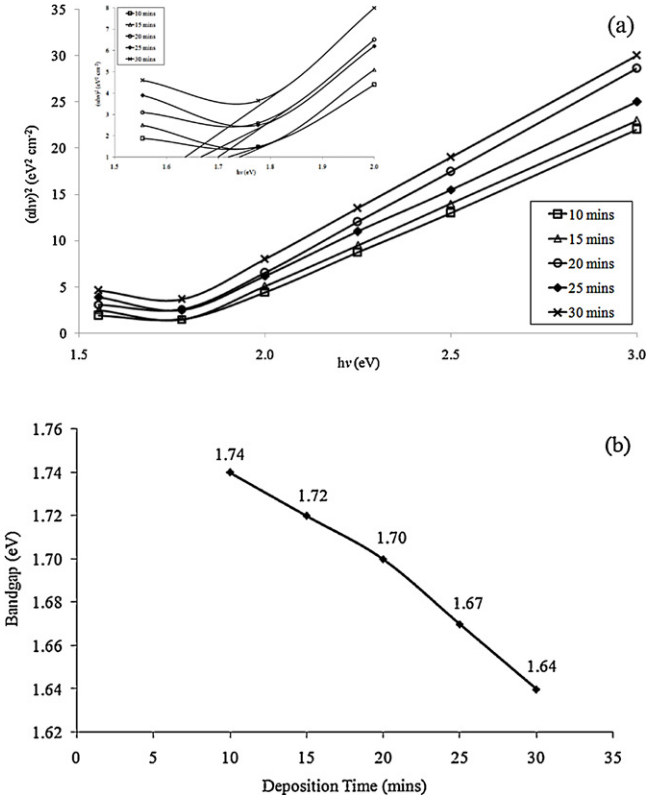

Fig. 11. Variation of MoS_2 thin films deposited at different deposition times. (a) $(\alpha h\nu)^2$ vs. $h\nu$ and (b) bandgap vs. deposition time.

Another important parameter to be deduced is the depletion layer width (W) and the band bending (V_b) that can be calculated from the relation:

$$V_b = V_{F,redox} - V_{FB}$$

$$W_{1/2} = \left(\frac{2\varepsilon\varepsilon_o V_b}{eN}\right) \quad (9)$$

where V_b is the built in voltage or the band bending and $V_{F,redox}$ is the redox potential of the $2I^-/I_2$ redox couple equal to $0.295V_{SCE}$ [22]. An expression for the density of states, N_c can be written as:

$$N_c = \frac{2}{h^3}(2\pi m_e^* kT)^{3/2} \quad (10)$$

where h is the Planck's constant (4.136×10^{-15} eV s), m_e is the effective electron mass in the conduction band and taken as $\approx 0.5m_e$ for molybdenum chalcogenides [28].

The measurement of capacitance as a function of applied voltage (i.e. Mott–Schottky plot) provides useful information such as the type of conductivity, flat band potential (V_{FB}) and depletion layer width, which could give an idea about the required semiconductor characteristics of MoSXSe2-X thin films that would be suitable to serve as PEC cell materials.

The flat band potential, V_{FB} of semiconductor is an important factor in explaining charge transfer process across the semiconductor–electrolyte junction of PEC cell. Since the band bending gives maximum possible output photovoltage from the semiconductor based device, it would be desirable from the stand point of efficiency to select redox systems such that $V_{F,redox}$ is close to E_v for n-type semiconductor photoanode based solar cells.

Theoretically, the conversion efficiency of a material varies with the material properties. Under light excitation, the maximum efficiency is given by [2]:

$$\eta_{max} = \frac{eV_b}{E_g} \quad (11)$$

where V_b is band bending and E_g is the energy gap (obtainable via Mott–Schottky plots and optical characterization). From the above expression it is evident that maximum efficiency depends upon the band bending and energy gap. Thus for a PEC cell, the larger the value of band bending, the greater will be the photoconversion efficiency. Therefore, the increased photoconversion efficiency with the increase of MoS_xSe_{2-x} film thickness is attributed to

(i) decrease in the band gap (E_g);
(ii) increase in the band bending, V_b of the material in films deposited at longer time (i.e. higher thickness).

Since the aim of the present work was to synthesize alloyed material in thin film form and to characterize it through the optical and electrical properties with special reference to the effect of the film composition and thickness, efforts to improve the efficiencies of the solar cells were not considered here.

The Mott–Schottky plot for of MoS_xSe_{2-x} ($0 \le x \le 2$) thin films is shown in Figs. 12–14 and their corresponding semiconductor parameters summarized in Tables 4–6, respectively. Intercepts of plots on voltage axis determine the flat band potential value of the junction. Fig. 12 shows the Mott–Schottky plot for $MoSe_2$ thin films at different deposition time. The values of semiconductor parameters obtained for the films are shown in Table 4. The flat band potential (V_{FB}) value is observed to decrease from −0.17 to −0.28 V as the deposition time increases. These values of V_{FB} for $MoSe_2$ deposited at 30 min are in good agreement with the value reported [30].

Fig. 13 shows the Mott–Schottky plot for MoSSe thin films at different deposition time. The results of the flatband potential and semiconductor parameters are shown. From the summary in Table 5, it is seen that the semiconductor parameter values for MoSSe is intermediate between $MoSe_2$ and MoS_2. This trend is in agreement with Gujarathi et al. [2] whereby they reported intermediate values for WS_xSe_{2-x} from the end members of the series WS_xSe_{2-x} (i.e. WSe_2 and WS_2). Fig. 14 shows the Mott–Schottky plot for MoS_2 thin films at different deposition time. The values of semiconductor parameters obtained for the films are shown in Table 6. It is seen that the values of V_{FB} MoS_2 deposited at 30 min are in good agreement with the values reported by Anand [31]. It

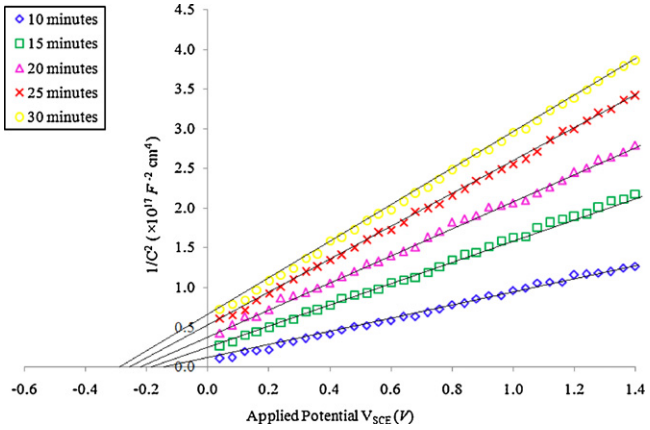

Fig. 12. Mott–Schottky plot for $MoSe_2$ thin films at different deposition time.

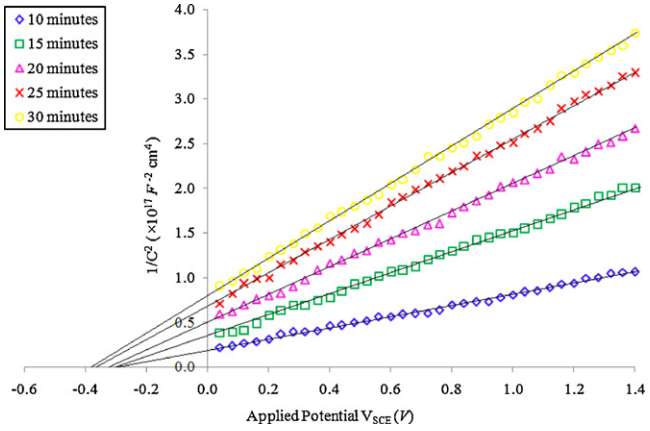

Fig. 13. Mott–Schottky plot for MoSSe thin films at different deposition time.

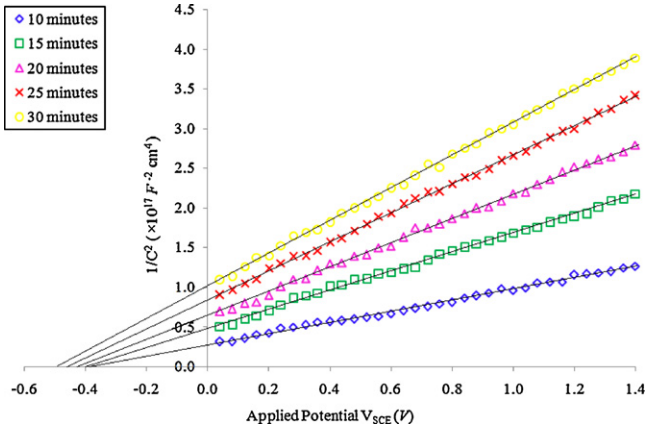

Fig. 14. Mott–Schottky plot for MoS_2 thin films at different deposition time.

Table 4
Summary of the results obtained from the Mott–Schottky plots for $MoSe_2$ films.

Semiconductor parameters	$MoSe_2$ thin film				
	10 min	15 min	20 min	25 min	30 min
Type of semiconductor	n	n	n	n	n
Flat band potential (V_{FB}) (V)	−0.17	−0.19	−0.22	−0.25	−0.28
Dielectric constant (ε)	44.1	39.0	37.3	34.1	33.5
Doping density (N) × 10^{29} (m^{-3})	1.83	1.40	1.10	0.83	0.72
Depletion layer width (W) (Å)	2.98	2.47	1.94	1.49	1.24
Density of states in Conduction Band (N_c) × 10^{13} (m^{-3})	4.196	4.196	4.196	4.196	4.196
Band bending (V_b) (V)	0.465	0.485	0.515	0.545	0.575
Energy gap (E_g) (eV)	1.22	1.20	1.17	1.15	1.12

Table 5
Summary of the results obtained from the Mott–Schottky plots for MoSSe films.

Semiconductor parameters	MoSSe thin film				
	10 min	15 min	20 min	25 min	30 min
Type of semiconductor	n	n	n	n	n
Flat band potential (V_{FB}) (V)	−0.29	−0.30	−0.33	−0.36	−0.38
Dielectric constant (ε)	41.0	32.4	30.5	29.5	30.1
Doping density (N) × 10^{29} (m^{-3})	1.65	1.09	0.84	0.68	0.57
Depletion layer width (W) (Å)	3.96	3.16	2.51	1.95	1.61
Density of states in Conduction Band (N_c) × 10^{13} (m^{-3})	4.196	4.196	4.196	4.196	4.196
Band bending (V_b) (V)	0.585	0.595	0.625	0.655	0.675
Energy gap (E_g) (eV)	1.66	1.61	1.54	1.50	1.44

Table 6
Summary of the results obtained from the Mott–Schottky plots for MoS_2 films.

Semiconductor parameters	MoS_2 thin film				
	10 min	15 min	20 min	25 min	30 min
Type of semiconductor	n	n	n	n	n
Flat band potential (V_{FB}) (V)	−0.39	−0.40	−0.42	−0.45	−0.48
Dielectric constant (ε)	35.8	29.3	28.7	27.7	27.4
Doping density (N) × 10^{29} (m^{-3})	1.39	0.97	0.75	0.57	0.48
Depletion layer width (W) (Å)	5.23	4.30	3.02	2.32	1.95
Density of states in Conduction Band (N_c) × 10^{13} (m^{-3})	4.196	4.196	4.196	4.196	4.196
Band bending (V_b) (V)	0.685	0.695	0.715	0.745	0.775
Energy gap (E_g) (eV)	1.74	1.72	1.7	1.67	1.64

was observed that flat band potential (V_{FB}) value to decrease from −0.39 to −0.48 V as the deposition time increases.

The nature of the Mott–Schottky plots as shown in Figs. 12–14 indicates that the MoS_xSe_{2-x} ($0 \le x \le 2$) films obtained are of n-type material. The values of different parameters obtained from the Mott–Schottky plots using equations (7) to (10) are summarised for all films respectively. For all films, the value of V_{FB} was found to decrease in thicker films. This is due to increase in crystallinity of the films in thicker films as proven by XRD results. The decreasing value of V_{FB} in the present investigation is attributed to lower band gap of the material in the thin film form as reported [32]. The value of V_{FB} is very important for solar cell applications because it determines the maximum possible cell photovoltage. The decreasing values for the depletion width of the films are in good agreement with the energy gap values retrieved from optical studies.

The dielectric constants for the films are also observed to decrease in thicker films. Although the dielectric constant for MoS_xSe_{2-x} ($0 \le x \le 2$) thin films decreases with time, this is a good trend because a higher dielectric constant is not necessarily desirable. Generally, substances with high dielectric constants break down more easily when subjected to intense electric fields, than do materials with low dielectric constants. Hence, the values obtained from the Mott–Schottky plots are accepted with good agreements with the reports given. With the compilation of the results on the semiconductor parameters, a comparison study was done to evaluate the suitability of the MoSSe thin films as a solar/PEC cell material. All values come in the range of many other transition metal chalcogenides and this has proven that MoS_xSe_{2-x} ($0 \le x \le 2$) thin films is capable as a solar/PEC cell material.

4. Conclusion

Results proved that MoS_xSe_{2-x} ($0 \le x \le 2$) thin films were successfully deposited on ITO-coated glass and stainless steel substrates. All films obtained were well adherent to the substrates with an 'ion-by-ion' growth mechanism. XRD analysis of the films proved polycrystalline MoSSe thin films with while EDX pattern confirmed that mixed combinatorial films of MoS_xSe_{2-x} ($0 \le x \le 2$) thin films have been formed through the electrodeposition process. Electron Microscope analysis confirmed the uniform and smooth nature of the films. Optical studies show the direct optical bandgap energy of the film. Results on the semiconductor parameters of the films revealed it is of n-type material and all semiconductor values come in the range of many other transition metal chalcogenides and this has proven that MoSSe thin films is capable as a solar/PEC cell material.

Acknowledgements

The work described in this paper was supported by Universiti Teknikal Malaysia Melaka (UTeM) and MoHE sponsored FRGS (Project No. FRGS/2011/FKP/TK 02/1 F00120).

References

[1] A.A. Yadav, E.U. Masumdar, Photoelectrochemical performances, of n-$CdS_{1-x}Se_x$ thin films prepared by spray pyrolysis technique, Solar Energy 84 (2010) 1445.
[2] D.N. Gujarathi, G.K. Solanki, M.P. Deshpande, M.K. Agarwal, PEC behaviour of mixed single crystals of tungsten sulphoselenide grown by a CVT technique, Solar Energy Materials and Solar Cells 90 (2006) 2630.
[3] A.V. Kokate, M.R. Asabe, S.D. Delekar, L.V. Gavali, I.S. Mulla, P.P. Hankare, B.K. Chougule, Photoelectrochemical properties of electrochemically deposited $CdIn_2S_4$ thin films, Journal of Physics and Chemistry of Solids 67 (2006) 2331.
[4] N. Romeo, A. Bosio, V. Canevari, A. Podesta, Recent progress on CdTe/CdS thin films for solar cells, Solar Energy 77 (2004) 795.
[5] R.A. Wibowo, W.S. Kim, E.S. Lee, B. Munir, K.H. Kim, Single step preparation of quaternary $Cu_2ZnSnSe_4$ thin films by RF magnetron sputtering from binary chalcogenide targets, Journal of Physics and Chemistry of Solids 68 (2007) 1908.
[6] J. Hernandez-Borja, Y.V. Vorobiev, R. Ramirez-Bon, Thin film solar cells of CdS/PbS chemically deposited by an ammonia-free process, Solar Energy Materials and Solar Cells 95 (2011) 1882.
[7] T.J.S. Anand, C. Sanjeeviraja, M. Jayachandran, Preparation of layered semiconductor ($MoSe_2$) by electrosynthesis, Vacuum 60 (2001) 431.
[8] P. Roy, S.K. Srivastava, Chemical bath deposition of MoS_2 thin film using ammonium tetrathiomolybdate as a single source for molybdenum and sulphur, Thin Solid Films 496 (2006) 293.
[9] Z. Zainal, N. Saravanan, H.L. Mien, Electrodeposition of nickel selenide thin films in the presence of triethanolamine as a complexing agent, Journal of Materials Science – Materials in Electronics 16 (2005) 111.
[10] K. Anuar, W.T. Tan, M.S. Atan, K. Dzulkefly, S.M. Ho, H. Md Jelas, N. Saravanan, Cyclic voltammetry study of copper tin sulfide compounds, Pacific Journal of Science and Technology 8 (2007) 252.
[11] S. Shariza, T.J.S. Anand, Effect of deposition time on the structural and optical properties of molybdenum chalcogenides thin films, Chalcogenide Letters 8 (2011) 529.
[12] P.P. Hankare, V.M. Bhuse, K.M. Garadkar, S.D. Delekar, I.S. Mulla, Low temperature route to grow polycrystalline cadmium selenide and mercury selenide thin films, Materials Chemistry and Physics 82 (2003) 711.
[13] B.D. Cullity, S.R. Stock, Elements of X-Ray Diffraction, Prentice Hall, 2001.
[14] K.R.M. Rao, S. Mukherjee, P.M. Raole, I. Manna, Characterization of surface microstructure and properties of low-energy high-dose plasma immersion ion-implanted 304L austenitic stainless steel, Surface and Coatings Technology 200 (2005) 2049.
[15] JCPDS Data File, Card No. 1-72-1420.
[16] JCPDS Data File, Card No. 1-71-6685.
[17] JCPDS Data File, Card No. 2-1133.
[18] Y. Chen, J. Wang, J. Lu, W. Zheng, J. Gu, S. Yang, X. Gao, Microcrystalline silicon grown by VHF PECVD and the fabrication of solar cells, Solar Energy 82 (2008) 1083.
[19] T.S. Sian, G.B. Reddy, Optical, structural and photoelectron spectroscopic studies on amorphous and crystalline molybdenum oxide thin films, Solar Energy Materials and Solar Cells 82 (2004) 375.
[20] B.D. Ajalkar, R.K. Mane, B.D. Sarwade, P.N. Bhosale, Optical and electrical studies on molybdenum sulphoselenide [$Mo(S_{1-x}Se_x)_2$] thin films prepared by arrested precipitation technique (APT), Solar Energy Materials and Solar Cells 81 (2004) 101.
[21] R.S. Patil, M.D. Uplane, P.S. Patil, Structural and optical properties of electrodeposited molybdenum oxide thin films, Applied Surface Science 252 (2006) 8050.
[22] C.D. Lokhande, B.R. Sankapal, R.S. Mane, H.M. Pathan, M. Muller, M. Giersig, V. Ganesan, XRD, SEM, AFM, HRTEM, EDAX and RBS studies of chemically deposited Sb_2S_3 and Sb_2Se_3 thin films, Applied Surface Science 193 (2002) 1.
[23] S. Srikanth, N. Suriyanarayanan, S. Prabahar, V. Balasubramanian, D. Kathirvel, Structural, Optical properties of chemical bath deposited Sb_2S_3 thin films, Advances in Applied Science Research 2 (2011) 95.
[24] A.V. Kokate, U.B. Suryavanshi, C.H. Bhosale, Structural, compositional, and optical properties of electrochemically deposited stoichiometric CdSe thin films from non-aqueous bath, Solar Energy 80 (2006) 156.
[25] M.M. Vora, A.M. Vora, Stacking faults in Re doped $MoSe_2$ single crystals, Chalcogenide Letters 5 (2008) 35.
[26] R.S. Patil, Electrosynthesis of the molybdenum disulphide thin films and characterization, Thin Solid Films 340 (1999) 11.
[27] J. Dheepa, R. Sathyamoorthy, A. Subbarayan, Optical properties of thermally evaporated Bi_2Te_3 thin films, Journal of Crystal Growth 274 (2005) 100.
[28] E. Guneri, C. Ulutas, F. Kirmizigul, G. Altindemir, F. Gode, C. Gumus, Effect of deposition time on structural, electrical, and optical properties of SnS thin films deposited by chemical bath deposition, Applied Surface Science 257 (2010) 1189.
[29] R.W. Miles, O.E. Ogah, G. Zoppi, I. Forbes, Thermally evaporated thin films of SnS for application in solar cell devices, Thin Solid Films 517 (2009) 4702.
[30] S. Chandra, D.P. Singh, P.C. Srivastava, S.N. Sahu, Electrodeposited semiconducting molybdenum selenide films: II. Optical, electrical, electrochemical and photoelectrochemical solar cell studies, Journal of Physics D: Applied Physics 17 (1984) 2125.
[31] T.J.S. Anand, Synthesis, Characterization of MoS_2 films for photoelectrochemical cells, Sains Malaysiana 38 (2009) 85.
[32] P.K. Pandey, N.S. Bhave, R.B. Kharat, Preparation and characterization of spray deposited $NiMoO_4$ thin films for photovoltaic electrochemical studies, Materials Research Bulletin 41 (2006) 1160.